# Actinide-to-Carbon Bonds in Cp₂An(alkyl)₂, -(butadiene), -(metallacyclopentadiene), and -(cyclobutadiene) Complexes

**Kazuyuki Tatsumi\* and Akira Nakamura\***

*Contribution from the Department of Macromolecular Science, Faculty of Science, Osaka University, Toyonaka, Osaka 560, Japan. Received November 17, 1986*

**Abstract:** The electronic structure of actinide bis(cyclopentadienyl)dialkyl, -butadiene, -metallacyclopentadiene, and -cyclobutadiene complexes is examined. Some $Cp*_2Th(alkyl)_2$ complexes display an interesting structural deformation in which a Th–C–C(alkyl) angle ($\alpha$) opens up considerably. A molecular orbital analysis of $Cp_2Th(C_2H_5)_2$ traces the deformation to the characteristic shape of the $d_\sigma$ fragment orbital of $Cp_2Th(C_2H_5)^+$. The potential energy curve for the ethyl pivoting was found to be very soft, with a shallow minimum at $\alpha \simeq 160°$. Nonrigidity of the ethyl orientation indicates that not only an $\alpha$ hydrogen but also a $\beta$ hydrogen can come close to Th without a loss of Th–C bond strength; the discussion should provide a theoretical basis for understanding important aspects of C–H activation chemistry involving actinide centers. The $Cp_2An(s\text{-}cis\text{-}C_4H_6)$ complex was calculated to be 0.74 eV (Th) or 0.42 eV (U) more stable than its $s\text{-}trans\text{-}C_4H_6$ isomer, in contrast to the analogous $Cp_2Zr(C_4H_6)$ complex where the stability of the two geometrical isomers was well-balanced. The $\sigma^2,\pi$ character of the $s\text{-}cis\text{-}C_4H_6$ coordination to An is somewhat less pronounced than that in the Zr congener, in harmony with the X-ray structures, while highly negative charges are accumulated on the $s\text{-}cis\text{-}C_4H_6$ terminal carbons. We noticed a strong An–C $\sigma$ interaction present in $Cp_2AnCH=CH\text{—}CH=CH$, but an An–C $\pi$ interaction was not well-developed. Although $Cp_2U(\eta^4\text{-}C_4H_4)$, an isomer of the metallacycle, is less stable by 2.5 eV, we point out that unknown cyclobutadiene complexes of actinides would be kinetically stable by the following two reasons: (1) the uranium-to-cyclobutadiene bonding itself is reasonably strong; and (2) an isomerization pathway to the energetically more favorable metallacycle is symmetry forbidden.

During the past decade organoactinide chemistry has undergone a period of rapid growth with an emphasis on thorium and uranium, and broad outlines of the behavior and descriptive chemistry of such 5f elements are emerging.[1,2] However, an understanding of the various facets of organoactinides is still far below the level of what we know about d-transition metal complexes. It remains a major challenge, both in the experimental arena and in the theoretical domain, to construct a logical framework that allows us to view factors determining fundamental chemical properties of 5f-transition metal compounds, e.g., molecular geometries and reactivity. We have applied the extended-Hückel MO method to this field[3-5] and have found the theoretical implications quite informative despite the approximate nature of the computational method. Our study is now extended to bis(cyclopentadienyl)actinide complexes with organic ligands with various bonding ca-

pabilities. While most of the actual molecules examined here carry pentamethylcyclopentadienyl ligands, they are replaced by nonsubstituted cyclopentadienyls for our calculations.

The present work was stimulated by recent synthetic achievements of $Cp*_2Th(CH_2CMe_3)_2$ (**1**)[6] and $Cp*_2An(1,3\text{-diene})$



**1**
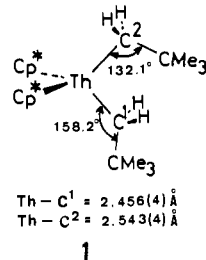
$(Cp^* = \eta^5\text{-}C_5Me_5; An = Th, U).$[7,8] There is little novel about the chemical formula of the former bisneopentyl complex, being one of a large body of Th(IV) compounds of the type $Cp*_2ThX_2$. However, the 50 K neutron diffraction study of **1** revealed an interesting coordination geometry at Th with highly unsymmetrical bonding of the neopentyl ligands.[6b] As shown below, the Th–C¹–C (neopentyl) angle is remarkably obtuse (158.2 (3)°) while coordination of the other neopentyl ligand is less distorted, ∠Th–C²–C = 132.1 (3)°. One might argue that the large Th–C¹–C angle would be a consequence of the severe steric congestion around the metal center. And yet, we should point out the rather short Th–C¹ distance which is even shorter than the Th–C² bond. Thus the Th atom is capable of holding tightly the unusual neopentyl coordination, and we wish to ask why it is so. The case is special, but we think that the structural information enshrines an important clue to a better understanding of actinide-to-alkyl bonds and their reactivity.

On the other hand, 1,3-dienes have shown variegated modes of coordination to d-transition metals, namely, classical s-cis $\eta^4$,

(1) (a) Marks, T. J.; Ernst, R. D. In *Comprehensive Organometallic Chemistry*; Wilkinson, G., Stone, F. G. A., Abel, E. W., Eds.; Pergamon Press: Oxford, 1982; Chapter 21. (b) Marks, T. J.; Fischer, R. D., Eds. *Organometallics of the f-Elements*; D. Reidel: Dordrecht, 1979. (c) Marks, T. J.; Fragalà, I. L., Eds. *Fundamental and Technological Aspects of Organo-f-Element Chemistry*; D. Reidel: Dordrecht, 1985.

(2) (a) Tsutsui, M.; Ely, M.; Dubois, R. *Acc. Chem. Res.* **1976**, *9*, 217-222. (b) Marks, T. J. *Ibid.* **1976**, *9*, 223-230. (c) Raymond, K. N.; Eigenbrot, C. W., Jr. *Ibid.* **1980**, *13*, 276-283. (d) Marks, T. J. *Science* **1982**, *217*, 989-997. (e) Marks, T. J. *Prog. Inorg. Chem.* **1979**, *25*, 224-333.

(3) (a) Tatsumi, K.; Hoffmann, R. *Inorg. Chem.* **1980**, *19*, 2656-2658. (b) Tatsumi, K.; Hoffmann, R. *Ibid.* **1984**, *23*, 1633-1634. (c) Tatsumi, K.; Nakamura, A. *J. Organomet. Chem.* **1984**, *272*, 141-154. (d) Cramer, R. E.; Mori, A. T.; Maynard, R. B.; Gilje, J. W.; Tatsumi, K.; Nakamura, A. *J. Am. Chem. Soc.* **1984**, *106*, 5920-5926. (e) Hofmann, P.; Stauffert, P.; Tatsumi, K.; Nakamura, A.; Hoffmann, R. *Organometallics* **1985**, *4*, 404-406. (f) Tatsumi, K.; Nakamura, A.; Hofmann, P.; Stauffert, P.; Hoffmann, R. *J. Am. Chem. Soc.* **1985**, *107*, 4440-4451. (g) Tatsumi, K.; Nakamura, A.; Hofmann, P.; Hoffmann, R.; Moloy, K. G.; Marks, T. J. *Ibid.* **1986**, *108*, 4467-4476. (h) Tatsumi, K.; Nakamura, A. In *Applied Quantum Chemistry*; Smith, V. H., Jr., Schaefer, H. F., III, Morokuma, K., Eds.; D. Reidel: Dordrecht, 1986; pp 299-311. (i) A short communication of this section has been published: Tatsumi, K.; Nakamura, A. *Organometallics* **1987**, *6*, 427-428.

(4) The extended Hückel method has been successfully applied also by J. V. Ortiz, J.-Y. Saillard, and R. Hoffmann for f-transition metal complexes: (a) Ortiz, J. V.; Hoffmann, R. *Inorg. Chem.* **1985**, *24*, 2095-2104. (b) Wrobleski, D. A.; Cromer, D. T.; Ortiz, J. V.; Rauchfuss, T. B.; Ryan, R. R.; Sattelberger, A. P. *J. Am. Chem. Soc.* **1986**, *108*, 174,175. (c) Rabaâ, H.; Saillard, J.-Y.; Hoffmann, R. *Ibid.* **1986**, *108*, 4327-4333.

(5) The $X_\alpha$-SW method has proved to be powerful in this area as well. For example, see: (a) Bursten, B. E.; Fang, A. *J. Am. Chem. Soc.* **1983**, *105*, 6495-6496. (b) Rösch, N.; Streitwieser, A., Jr. *Ibid.* **1983**, *105*, 7237-7240. (c) Hohl, D.; Rösch, N. *Inorg. Chem.* **1986**, *25*, 2711-2718.

(6) (a) Fagan, P. J.; Manriquez, J. M.; Maatta, E. A.; Seyam, A. M.; Marks, T. J. *J. Am. Chem. Soc.* **1981**, *103*, 6650-6667. (b) Bruno, J. W.; Smith, G. M.; Marks, T. J.; Fair, C. K.; Schultz, A. J.; Williams, J. M. *Ibid.* **1986**, *108*, 40-56.

(7) Smith, G. M.; Suzuki, H.; Sonnenberger, D. C.; Day, V. W.; Marks, T. J. *Organometallics* **1986**, *5*, 549-561.

(8) (a) Erker, G.; Mühlenbernd, T.; Benn, R.; Rufińska, A. *Organometallics* **1986**, *5*, 402-404. (b) Mühlenbernd, T.; Erker, G., private communication.

**Table I.** Atomic Parameters Used for Extended-Hückel Calculations

| atom | orbital | $H_{ii}$, eV | exponent[a] |
|------|---------|---------|-------------|
| Th | 7s | −5.39 | 1.834 |
|    | 7p | −5.39 | 1.834 |
|    | 6d | −10.11 | 2.461 (0.7612) + 1.165 (0.4071) |
|    | 5f | −9.64 | 4.477 (0.7682) + 1.837 (0.4267) |
|    | 6p | −27.83 | 3.806 |
| U | 7s | −5.50 | 1.914 |
|   | 7p | −5.50 | 1.914 |
|   | 6d | −9.19 | 2.581 (0.7608) + 1.207 (0.4126) |
|   | 5f | −10.62 | 4.943 (0.7844) + 2.106 (0.3908) |
|   | 6p | −30.03 | 4.033 |
| Ti | 4s | −8.97 | 1.075 |
|    | 4p | −5.44 | 0.675 |
|    | 3d | −10.81 | 4.55 (0.4206) + 1.40 (0.7839) |
| Nb | 5s | −10.95 | 1.89 |
|    | 5p | −7.59 | 1.85 |
|    | 4d | −13.23 | 4.08 (0.6401) + 1.64 (0.5516) |
| C | 2s | −21.40 | 1.625 |
|   | 2p | −11.40 | 1.625 |
| H | 1s | −13.60 | 1.300 |

[a]The numbers in parentheses are contraction coefficients used in the double-$\zeta$ expansion.

**Table II.** $A$, $B$, and $C$ Parameters of 6d and 5f Orbitals of Th and U for Charge-Iterative Calculations (in eV)

|    |    | $A$ | $B$ | $C$ |
|----|----|-----|-----|-----|
| Th | 6d | −0.874 | −3.46 | −2.89 |
|    | 5f | −1.01 | −3.66 | −1.80 |
| U  | 6d | −0.906 | −3.62 | −2.89 |
|    | 5f | −1.02 | −3.89 | −3.77 |

s-cis 1,4-$\eta^2$ (or $\sigma^2,\pi$), 1,2-$\eta^2$, or s-trans $\eta^4$, depending on the choice of a metal atom and auxiliary ligands. And we may use various stages of 1,3-diene coordination geometries as a measure of bonding ability of metal fragment partners. Thus the syntheses of Cp*$_2$An(1,3-diene) and the concomitant structure determination of Cp*$_2$Th(C$_4$H$_6$) (**2**) provided us with another good opportunity



Th−C$^{1,4}$ = 2.54(2), 2.60(3) Å
Th−C$^{2,3}$ = 2.73(2), 2.74(3) Å

**2**
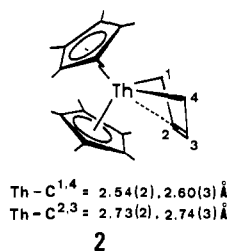
to examine properties of actinide–carbon bonding being weighed against d metal analogues.

This theoretical contribution includes also an analysis for metallacyclopentadiene, Cp$_2$AnCH=CH—CH=CH. The study will then prompt us to propose that there is a chance to isolate as yet unknown cyclobutadiene complexes of actinides, e.g., Cp$_2$An($\eta^4$-C$_4$H$_4$) which is an isomer of Cp$_2$AnCH=CH—CH=CH. Our investigations here follow a familiar strategy: the fragment orbitals of Cp$_2$Th$^{2+}$ and Cp$_2$U$^{2+}$ are first constructed, and then they are used as a basis for the description of the bonding with different ligands in question.

**Calculational Details**

All the calculations were based on the extended-Hückel method.[9] Atomic radial wave functions of the actinide 6d and 5f orbitals are of Slater-type with double-$\zeta$ quality, while the 7s, 7p, and 6p orbitals are of single-$\zeta$ type. Exponents of these orbitals were estimated as follows from the relativistic Dirac–Fock wave functions reported by Desclaux.[10] In determining the double-$\zeta$ parameters of U 6d and 5f, we used $R_{max}$, radius of maximum radial density, $\langle r \rangle$, and $\langle r^2 \rangle$ of U 6d$_{5/2}$ and 6d$_{3/2}$, and those of U 5f$_{7/2}$ and 5f$_{5/2}$, respectively. The relativistic functions were transformed to quasi-relativistic 6d and 5f orbitals[11] by taking weighted averages of each multiplet. Thus spin–orbit splittings do not appear in our basis sets, although the other relativistic effects within a uranium atom remain implicitly intact. For the single-$\zeta$-type U 7s and 7p orbitals, the exponents were estimated from $R_{max}$ of the U 7s$_{1/2}$

function, while $R_{max}$ of U 6p$_{1/2}$ was used for our quasi-relativistic U 6p orbitals.

The Desclaux's relativistic functions of Th have been given assuming the 7s$^2$6d$^2$ electronic configuration which differs from the 7s$^2$6d$^1$5f$^n$-type configurations used for the elements, Pa ($n$ = 2), U ($n$ = 3), and Np ($n$ = 4). Since we wanted to maintain the broad trend of the actinide series, the Th orbital exponents were not determined directly from the Desclaux's Th functions but were obtained by quadratic extrapolation of the corresponding Np, U, and Pa parameters. The resulting exponents for Th and U are summarized in Table I.

The diagonal terms, $H_{ii}$, for U 7s, 7p, and 6p orbitals were also taken from the orbital energies of the Desclaux's functions, and those for Th were again quadratically extrapolated in the series Np → U → Pa → Th. For $H_{ii}$'s of 6d and 5f orbitals, we introduced the charge consistent approach.[12] The diagonal element was then approximated as a parabolic function of the atomic charge $Q$ in terms of the Mulliken population analysis. The Madelung corrections, which may account for interatomic electron repulsions, were neglected according to the standard extended Hückel procedure of Hoffmann and collaborators. The $A$, $B$, and $C$ parameters were determined based on the Dirac–Slater atomic orbital energies for the neutral 7s$^2$6d$^1$5f$^n$, the monocationic 7s$^1$6d$^1$5f$^n$, and the dicationic 7s$^0$6d$^1$5f$^n$ configurations. The Dirac–Slater atomic calculations were done using the relativistic X$_\alpha$ program of Liberman et al.,[13] with the fixed $\alpha$ value of 0.72. Table II lists the $A$, $B$, and $C$ parameters for the 6d and 5f orbitals of Th and U.

$$H_{ii} = AQ^2 + BQ + C \qquad (1)$$

The charge-iterative calculations were performed on Cp$_2$Th($s$-$cis$-C$_4$H$_6$) and Cp$_2$U($s$-$cis$-C$_4$H$_6$) ($L$ = 0.5 Å and $\theta$ = 30°), where the geometrical variables $L$ and $\theta$ will be described later in the text. The final $H_{ii}$ values so obtained for 6d and 5f orbitals are then used as fixed parameters for calculations throughout this paper. The extended-Hückel parameters for Ti, Nb, C, and H are the same as in other works.[14] These are collected in Table I. The off-diagonal elements $H_{ij}$ were calculated by a weighted Wolfsberg–Helmholtz formula with the standard $K$ value of 1.75.[15]

Geometrical parameters not described in the following sections are as follows. Cp$_2$Th(C$_2$H$_5$)$_2$: Th–Cp centroid, 2.55 Å; Cp–Th–Cp, 133°; Th–C(C$_2$H$_5$), 2.50 Å; C–C(C$_2$H$_5$), 1.56 Å; C–H, 1.09 Å; C–C(Cp), 1.42 Å. Cp$_2$Nb(C$_2$H$_5$)(CH$_2$=CH$_2$): Nb–Cp centroid, 2.10 Å; Cp–Nb–Cp, 132°; C–C(Cp), 1.38 Å; Nb–C(C$_2$H$_5$), 2.32 Å; Nb–C(C$_2$H$_4$), 2.30 Å; C–C(C$_2$H$_4$), 1.41 Å; x–Nb–C(C$_2$H$_5$), 46.3°; x–Nb–C$_2$H$_4$ centroid, 46.3°. Cp$_2$An(C$_4$H$_6$)(An = Th, U): An–Cp centroid, 2.58 Å; Cp–An–Cp, 132°; C–C(CP), 1.42 Å; C–C(C$_4$H$_6$), 1.44 Å. Cp$_2$UC$^1$HC$^2$HC$^3$HC$^4$H: U–C$^{1,4}$, 2.45 Å; C$^1$–C$^2$, 1.37 Å; C$^2$–C$^3$, 1.45 Å; C–C–C, 120°; C–C–H, 120°. Cp$_2$ThC$^1$HC$^2$HC$^3$HC$^4$H: Th–C$^{1,4}$, 2.50 Å. Cp$_2$TiC$^1$HC$^2$HC$^3$HC$^4$H: Ti–C$^{1,4}$, 2.15 Å; Ti–Cp centroid, 2.06 Å; Cp–Ti–Cp, 132°. Cp$_2$U($\eta^4$-C$_4$H$_4$): U–C(C$_4$H$_4$), 2.60 Å; C–C(C$_4$H$_4$), 1.44 Å.

**Cp$_2$An Fragment Orbitals**

Molecular orbitals of a bent Cp$_2$Ti fragment were examined in detail by Brintzinger and Bartell[16] and also by Lauher and

(9) (a) Hoffmann, R. *J. Chem. Phys.* **1963**, *39*, 1397–1412. (b) Hoffmann, R.; Libscomb, W. N. *Ibid.* **1962**, *36*, 2179–2189.

(10) Desclaux, J. P. *At. Data Nucl. Data Tables* **1973**, *12*, 311–406.

(11) These basis sets were previously reported by us as nonrelativistic atomic orbitals, but the notation, "quasi-relativistic", used in this paper should be more appropriate. See ref 3a.
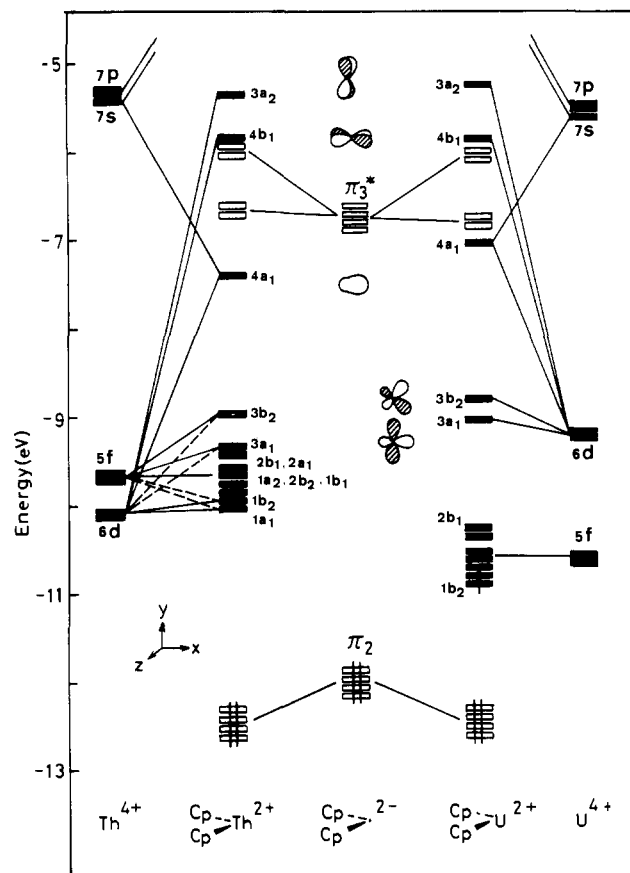
(12) The charge-iterative version of the REX (relativistically parametrized extended Hückel) method has been successfully applied to some actinide complexes by: Larsson, S.; Pyykkö, P. *Chem. Phys.* **1986**, *101*, 355–369.

(13) Liberman, D. A.; Cromer, D. T.; Waber, J. T. *Comput. Phys. Commun.* **1971**, *2*, 107–111. The Dirac–Slater atomic calculations were done during the K.T.'s visit at University of Helsinki, fall 1985; K. T. thanks P. Pyykkö for his hospitality. Parametrization for the charge-iterative version of the REX method using the same philosophy will be given separately: Pyykkö, P.; Tatsumi, K., manuscript in preparation.

(14) (a) Lauher, J. W.; Hoffmann, R. *J. Am. Chem. Soc.* **1976**, *98*, 1729–1742. (b) Tatsumi, K.; Hoffmann, R. *Ibid.* **1981**, *103*, 3328–3341.

(15) Ammeter, J. H.; Burgi, H.-B.; Thibeault, J. C.; Hoffmann, R. *J. Am. Chem. Soc.* **1978**, *100*, 3686–3692. See also ref 3g.

(16) Brinzinger, H. H.; Bartell, L. S. *J. Am. Chem. Soc.* **1970**, *92*, 1105–1107.

**Figure 1.** Interaction diagrams for $Cp_2Th^{2+}$ (left) and $Cp_2U^{2+}$ (right). The actinide 6p as well as the cyclopentadienyl $\pi_1$ orbitals are low in energy and are not shown in the figure.

Hoffmann.[17] They brought us a substantial understanding of the chemistry of ubiquitous $Cp_2ML_n$ complexes of d elements in all its aspects. Recently molecular orbitals of the lanthanide congeners $Cp_2Sm$ and $Cp_2Lu$ have also appeared.[4a,c] There may, indeed, be some similarity between these $Cp_2M$ fragments and $Cp_2An$, but it is perhaps of use to give a full account of the $Cp_2Th^{2+}$ and $Cp_2U^{2+}$ fragment orbitals now in order to show how they are similar and/or different from each other.

In a bent $C_{2v}$ geometry, the $\pi$ orbitals of two $Cp^-$ ligands give familiar three sets of nearly degenerate orbitals arising from $Cp^-$ $\pi_1$, $\pi_2$, and $\pi_3^*$. Figure 1 shows interactions between these and the $Th^{4+}$ and $U^{4+}$ orbitals, where the low-lying $Cp$ $\pi_1$ levels at $\sim -14.4$ to $-14.3$ eV as well as still lower $Th(U)$ 6p levels at $-27.8$ eV ($-30.0$ eV) are omitted for clarity. The actinide 7s, 7p, and 6d orbitals all move up in energy by different amounts as they interact with $Cp$ $\pi$ orbitals, in which the strongly destabilized s and p orbitals are outside the energy range of Figure 1. The high-lying $3a_2$ and $4b_1$ of both $Cp_2Th^{2+}$ and $Cp_2U^{2+}$ consist primarily of actinide $yz$ and $xz$, respectively,[18] and four levels of mostly $Cp$ $\pi^*_3$ in character are located right below them. At slightly lower energy, $4a_1$ is a hybrid of s (26% for Th, 27% for U), $x$ (12%, 12%), $x^2 - y^2$ (2%, 2%), and $z^2$ (53%, 55%). In the energy region of $-9 \sim -11$ eV there are nine molecular orbitals made of 6d and 5f. For $Cp_2U^{2+}$ d–f mixing is not large so that $3b_2$ and $3a_1$ are recognized as chiefly d orbitals with a slight admixture of p and f, the main lobes of which settle in the equatorial girdle ($xy$ plane) of $Cp_2U^{2+}$. The composition of these orbitals is $y$ (6%) + $xy$ (71%) – $yz^2$ (3%) for $3b_2$ and s (1%) +

---

(17) See ref 14a. The following papers describe the bent $Cp_2M$ fragment orbitals for other metals: Brinzinger, H. H.; Lohr, L. L., Jr.; Wong, K. L. T. *J. Am. Chem. Soc.* **1975**, *97*, 5146–5155. Petersen, J. L.; Lichtenberger, D. L.; Fenske, R. F.; Dahl, L. F. *Ibid.* **1975**, *97*, 6433–6441 and references therein.

(18) Note that the coordination system chosen for the $Cp_2An^{2+}$ fragments in Figure 1 and throughout this paper differs from the one used in ref 14a.



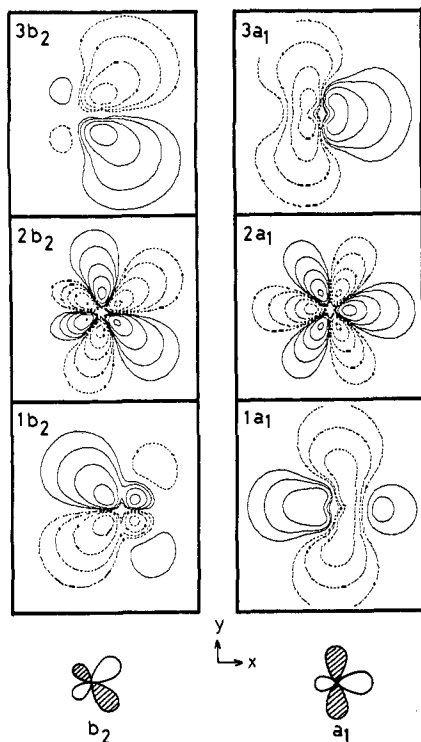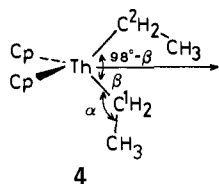**Figure 2.** Contour plots of the important valence orbitals in a $Cp_2U^{2+}$ fragment. From top to bottom: $4b_1$, $4a_1$, $3b_2$, and $3a_1$. The contour levels of each diagram are $\pm 0.025$, $\pm 0.05$, $\pm 0.1$, and $\pm 0.2$.

$x$ (3%) + $z^2$ (5%) + ($x^2 - y^2$) (73%) – $xz^2$ (1%) for $3a_1$. Thus the remaining seven orbitals, $1b_2$ – $2b_1$, are dominantly f in character. In the case of $Cp_2Th^{2+}$, the corresponding nest of nine orbitals suffer from strong d–f mixing, because the Th 6d and 5f levels are energetically close in our parametrization.

In most $Cp_2AnL_n$ complexes, coordination of L's occurs in the equatorial $xy$ plane, and so the frontier orbitals of $Cp_2An^{2+}$ which will play a prime role in bonding are those having extent in that plane. The $4a_1$, $3b_2$, and $3a_1$ orbitals of $Cp_2U^{2+}$ fall obviously in this category, and their computed shapes are illustrated in Figure 2. The contour plot of $4b_1$ is also given, which lies perpendicular to the equatorial plane and contribute to $\pi$ interactions, if any, with L's. One may notice that these orbitals closely resemble, in appearance, the corresponding frontier orbitals of $Cp_2Ti^{2+}$.[14a] However, the $Cp_2U^{2+}$ orbitals are about 2 eV higher in energy and are more diffuse than the $Cp_2Ti^{2+}$ orbitals. The character of $3a_1$ is somewhat different as well, in such a way that the orbital lobe pointing in the direction of $+x$ is as large as those in the $\pm y$ direction, in contrast to the nearly pure $y^2$ character of $Cp_2Ti^{2+}$ $a_1$, **3**. These differences, albeit seemingly subtle, will become



**3**
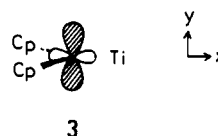
important in assessing bonding capability characteristic of $Cp_2U^{2+}$ and $Cp_2Th^{2+}$.

For $Cp_2Th^{2+}$, the d-orbital character analogous to $3b_2$ or $3a_1$ of $Cp_2U^{2+}$ is scattered in the group of nine levels resulting in complicated d–f hybridization. Of them, those having $a_1$ or $b_2$ symmetry contain contributions from such d character, to one degree or another. Figure 3 shows their contour plots. The $2b_2$ and $2a_1$ orbitals are easily recognized as $y(3x^2 - y^2)$ and $x(x^2 -$

**Figure 3.** Contour plots of the $a_1$ and $b_2$ symmetry orbitals in the nest of low-lying vacant orbitals in a $Cp_2Th^{2+}$ fragment.



**Figure 4.** Potential energy curves of $Cp_2Th(C_2H_5)_2$ and $Cp_2Nb(H_2C=CH_2)(C_2H_5)$ as a function of M–C–C(ethyl) angle $\alpha$. The experimentally observed angle $\alpha$ for $Cp*_2Th(CH_2CMe_3)_2$ or $Cp_2Nb(H_2C=CH_2)(C_2H_5)$ is located by a mark "exp." in each corresponding curve.

$3y^2$) from their orbital shapes, of which $2b_2$ carries a small d component of 13%. Although the contour maps of $Cp_2Th^{2+}$ $3b_2$ and $3a_1$ appear to be similar to the $Cp_2U^{2+}$ $3b_2$ and $3a_1$ orbitals, the net d contribution is larger for $1b_2$ and $1a_1$, be they 24% ($3b_2$), 21% ($3a_1$), 39% ($1b_2$), and 60% ($1a_1$). It should be noted here that the strong d–f hybridization in these levels is not an important phenomenon by itself as far as Th–L bonding is concerned. When an equatorial ligand(s) L approaches, the d component in each hybrid orbital tends to interact with the ligand more strongly than the f component. Then dehybridization usually takes place, as will be shown in the following sections, leaving seven levels of predominantly f character at relatively low energy. Therefore, the bonding capability of $Cp_2Th^{2+}$ does not differ much from that of $Cp_2U^{2+}$, except that the Th valence orbitals are more diffuse than the U orbitals and the 5f levels are higher for Th while the 6d levels are lower. The trends may be seen explicitly in our extended-Hückel parameters listed in Table I.

## Unusual Th–C–C Angle in $Cp*_2Th(CH_2CMe_3)_2$[31]

The question was raised earlier as to why one of the Th–C–C (neopentyl) angles opens up to 158.2° in $Cp*_2Th(CH_2CMe_3)_2$ (1) or how the Th atom forms a strong bond with the distorted neopentyl ligand. We now examine the question using a simplified model compound, $Cp_2Th(C_2H_5)_2$. Exploratory calculations were carried out by varying the Th–$C^1$–C angle $\alpha$ and $x$–Th–$C^1$ angle $\beta$ independently, as shown in **4**. The local tetrahedral geometry



**4**

at $C^1$ was retained, so that $C^1H_2CH_3$ rocks as a rigid group when $\alpha$ is varied. Also fixed were the Th–$C^2$–C angle of 132.1° and the $C^1$–Th–$C^2$ angle of 98°, which were taken from the X-ray structure of **1**. For a wide range of $\alpha$, the optimized $\beta$ was found to be nearly constant at 50°. Therefore, Figure 4 shows the potential energy curve as a function of $\alpha$, with $\beta = 50°$. We have calculated also the potential curve for bending of the ethyl group
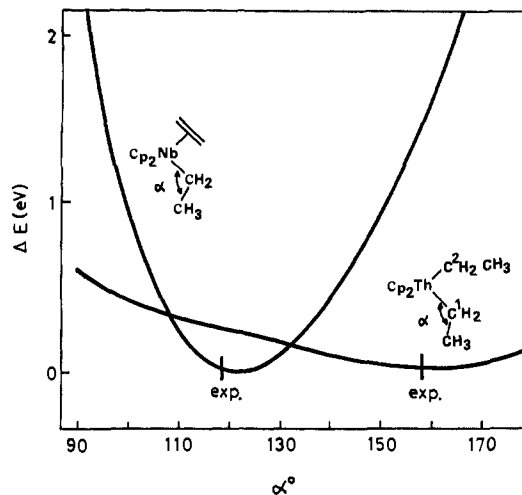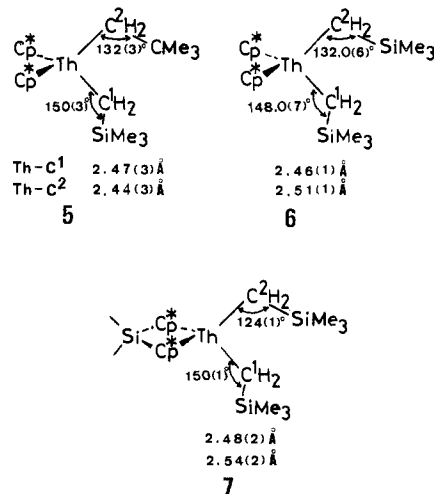
in the typical d-metal congener, $Cp_2Nb(H_2C=CH_2)(C_2H_5)$,[19] for comparison. The variational parameter is then the Nb–C–C(ethyl) angle $\alpha$. The result is superimposed on the Th curve in Figure 4.

For the Nb complex, the energy minimum appears at $\alpha = 121°$, in good accordance with the experimentally observed angle, $\alpha = 118.6$ (7)°. The optimal geometry of $Cp_2Nb(H_2C=CH_2)(C_2H_5)$ may well represent a "normal" alkyl coordination to a metal center. On the other hand, the Th complex has a soft curve. A shallow minimum comes at about $\alpha = 160°$, which we will term the "distorted" geometry hereafter. The calculated potential energy curve indicates that the mode of ethyl coordination to Th is not very rigid in harmony with the NMR data for **1**.[6b] For example, moving the ethyl group from the favorable distorted geometry to the less distorted coordination geometry ($\alpha = 130$ or 120°) costs relatively little energy: 0.16 eV (3.7 kcal/mol) or 0.23 eV (5.3 kcal/mol). A variety of bending angles $\alpha$ would be electronically plausible, and an optimum may be determined by small electronic and/or steric perturbation. Nevertheless, it is encouraging to find that the calculated Th–$C^1$–C angle for $Cp_2Th(C_2H_5)_2$ agrees satisfactorily with the neutron-derived structure of **1**.

There are three homologues of **1**: $Cp*_2Th(CH_2CMe_3)$-$(CH_2SiMe_3)$ (5),[6] $Cp*_2Th(CH_2SiMe_3)_2$ (6),[20a] and $(CH_3)_2Si$-$\{(CH_3)_4C_5\}_2Th(CH_2SiMe_3)_2$ (7).[20b] Each molecule is charac-



Th–$C^1$   2.47(3) Å
Th–$C^2$   2.44(3) Å

**5**

Th–$C^1$   2.46(1) Å
Th–$C^2$   2.51(1) Å

**6**



2.48(2) Å
2.54(2) Å

**7**

(19) Guggenberger, L. J.; Meakin, P.; Tebbe, F. N. *J. Am. Chem. Soc.* **1974**, *96*, 5420–5427.

(20) (a) Bruno, J. W.; Marks, T. J.; Day, V. W. *J. Organomet. Chem.* **1983**, *250*, 237–246. (b) Fendrick, C. M.; Mintz, E. A.; Schertz, L. D.; Marks, T. J.; Day, V. W. *Organometallics* **1984**, *3*, 819–821.
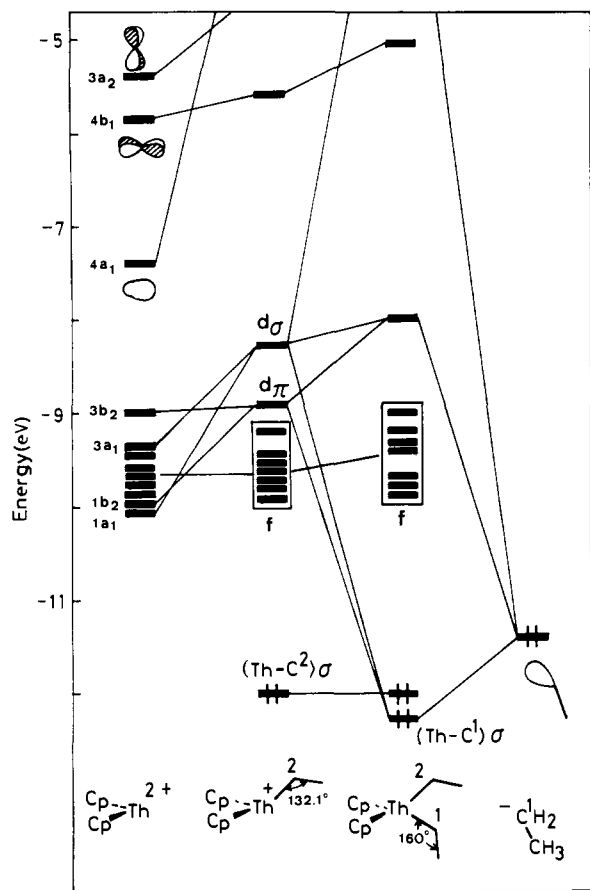
*Bis(cyclopentadienyl)actinide Complexes*

*J. Am. Chem. Soc., Vol. 109, No. 11, 1987* 3199



**Figure 5.** Construction of the orbitals of $Cp_2Th(C_2H_5)_2$. From left to right: the $Cp_2Th^{2+}$ fragment orbitals, the orbitals of $Cp_2Th(C^2H_2CH_3)^+$, and then such orbitals allowed to interact with the $\sigma$ donor orbital of a deformed $C^1H_2CH_3^-$ ligand, shown at the extreme right.

terized by the one large Th–C–Si angle which is reminiscent of the distorted neopentyl coordination in **1**. The Th–C$^1$–Si angles ($\sim$150°) are slightly smaller than the Th–C$^1$–C angle of **1**, yet they are reasonably close to the potential minimum computed for $Cp_2Th(C_2H_5)_2$. In **6** and **7**, the obtuse Th–C$^1$–Si angles are again accompanied by shortened Th–C$^1$ bond distances, being 2.46 and 2.48 Å. Although we cannot simply compare the Th–C distances of the nonequivalent alkyl ligands in **5**, the Th–C$^1$ length of 2.47 Å indicates that probably similar bond shortening persists in this molecule as well.

Perhaps not unrelated to such distortions is an unusual mode of $CH(SiMe_3)_2$ coordination to Nd in $Cp^*_2NdCH(SiMe_3)_2$[21] and in $(CH_3)_2Si\{(CH_3)_4C_5\}_2NdCH(SiMe_3)_2$ (**8**).[22] Surprisingly, atoms



**8**
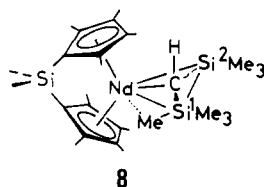
Nd, C, Si,$^1$ and Si$^2$ are coplanar to within 0.02 (1) Å for the former complex and 0.04 (1) Å for the latter and thus the Nd–C–H angle is acute ($\sim$76°). Another interesting aspect of the Nd complexes is the highly unsymmetrical interaction of the $CH(SiMe_3)_2$ ligand with Nd. The alkyl group pivots in place as shown in **8** so that a small Nd–C–Si$^1$ angle, down to 96.7 (3)° for **8** or 98.4 (3)° for the $Cp^*_2Nd$ analogue, and a concomitant large Nd–C–Si$^2$ angle,

up to 132.4 (4)° or 140.2 (4)°, are seen. These interesting observations await theoretical studies, but regrettably we do not go into them in the present paper.

In contrast to **1** and **5–7**, $Cp_3UR$ complexes so far obtained do not show a significant alkyl distortion: $\angle U$–C–C = 128.5 (16)° ($Cp_3U(n\text{-}Bu)$),[23a] 120 (1)° ($Cp_3U(n\text{-}Bu)^-$),[23b] 128.6 (9)° ($Cp_3U$-($p\text{-}CH_3C_6H_4CH_2$)),[23a] and 127 (4)° ($Cp_3U(\sigma\text{-}CH_2CMeCH_2)$).[24] On the other hand, a benzyl group in $Th(CH_2Ph)_4$-($Me_2PCH_2CH_2PMe_2$) is coordinated to Th with acute Th–C–C angles (88 (1) and 90 (1)°), while in $U(CH_2Ph)_3Me$-($Me_2PCH_2CH_2PMe_2$) two U–C–C angles are small (97.7 (4) and 83.0 (4)°),[25] probably because the phenyl $\pi$ system is interacting with Th or U.

The molecular orbitals for $Cp_2Th(C_2H_5)_2$ ($\alpha$ = 160°) are constructed in Figure 5 by stepwise additions of two ethyls to the $Cp_2Th^{2+}$ fragment. When $Cp_2Th^{2+}$ is allowed to interact with the $C^2H_2CH_3^-$ ligand on the left side of the figure, $4a_1$, $4b_1$, and $3a_2$ are destabilized to varying degrees. At the same time, the strong d–f mixing in the low-lying nine orbitals of $Cp_2Th^{2+}$ is dissolved, and they split into an f block and two higher levels, largely d in character. According to the contour plots shown in **9** and **10**, the two d orbitals are locally of $\sigma$ and $\pi$ types with





**9**          **10**
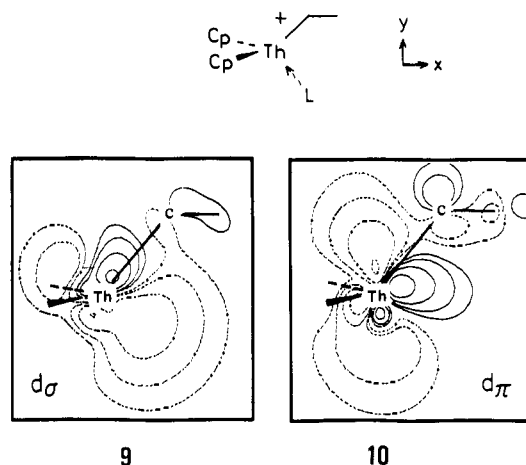
respect to an incoming ligand L, the second ethyl group $C^1H_2CH_3^-$ in this case. Thus they are named $d_\sigma$ and $d_\pi$, respectively.[3f] In addition, there appears a Th–C$^2$ $\sigma$ bonding orbital at –12.0 eV.

Next the interaction with the distorted $C^1H_2CH_3^-$ ligand is introduced in Figure 5, right. Because of the large Th–C$^1$–C angle ($\alpha$ = 160°), $d_\sigma$ and $d_\pi$ of $Cp_2Th(C^2H_2CH_3)^+$ both overlap with the donor orbital of $C^1H_2CH_3^-$, setting up the (Th–C$^1$) $\sigma$ bonding molecular orbital. As it happens, the (Th–C$^2$) $\sigma$ level is undisturbed by this interaction and stays put. As a consequence, (Th–C$^1$) $\sigma$ does not contain a notable contribution from the $C^2H_2CH^-$ lone-pair orbital in this low molecular symmetry. The contour plots of these occupied $\sigma$ orbitals are shown in **11** and **12**, where the composition of the Th valence orbitals is 7p (6%) + 6d (2%) + 5f (5%) (**11**) or 7p (5%) + 6d (7%) + 5f (3%) (**12**). Evidently the Th–C$^1$ bonding interaction is well-retained, or at least as good as the Th–C$^2$ $\sigma$, in spite of the highly distorted mode of the $C^1H_2CH_3^-$ coordination.

An interesting aspect of the interaction diagram of Figure 5 is that the (Th–C$^1$) $\sigma$ level (**12**) is slightly lower than the (Th–C$^2$) $\sigma$ level (**11**) for the distorted geometry ($\alpha$ = 160°). It proves the presence of a stable Th–C$^1$ bond as was witnessed in the contour map of **12**. At $\alpha$ = 120°, the two $\sigma$ levels were found to be approximately degenerate. As $\alpha$ opens up, (Th–C$^1$) $\sigma$ moves down in energy, while (Th–C$^2$) $\sigma$ is left alone, resulting in the energy gap of 0.28 eV at $\alpha$ = 160°. The stabilization of the (Th–C$^1$)

(21) (a) Mauermann, H.; Swepston, P. N.; Marks, T. J. *Organometallics* **1985**, *4*, 200–202. (b) Jeske, G.; Lauke, H.; Mauermann, H.; Swepson, P. N.; Schumann, H.; Marks, T. J. *J. Am. Chem. Soc.* **1985**, *107*, 8091–8103.

(22) Jeske, G.; Schock, L. E.; Swepston, P. N.; Schumann, H.; Marks, T. J. *J. Am. Chem. Soc.* **1985**, *107*, 8103–8110.

(23) (a) Perego, G.; Cesari, M.; Farina, F.; Lugli, G. *Acta Crystallogr.*, *Sect. B* **1976**, *32*, 3034–3039. (b) Arnaudet, L.; Charpin, P.; Folcher, G.; Lance, M.; Nierlich, M.; Vigner, D. *Organometallics* **1986**, *5*, 270–274.

(24) Halstead, G. W.; Baker, E. C.; Raymond, K. N. *J. Am. Chem. Soc.* **1975**, *97*, 3049–3052.

(25) Edwards, P. G.; Andersen, R. A.; Zalkin, A. *Organometallics* **1984**, *3*, 293–298.

Th–C$^2$ σ                    Th–C$^1$ σ

**11**                              **12**
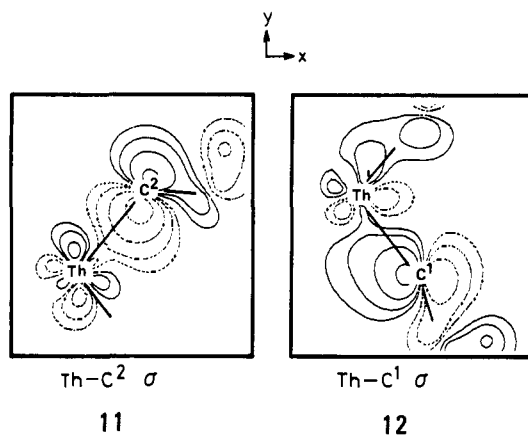
σ molecular orbital is the main reason why the potential curve in Figure 4 moves down as the C$^1$H$_2$CH$_3$ ligand tends to distort.

When C$^1$H$_2$CH$_3$ is not tilted much ($\alpha$ = 120–130°), it is clear from **9** that the ethyl group is bound to Th primarily through an interaction with d$_\sigma$. Distortion weakens this interaction, but not very much, since the main lobe of d$_\sigma$ is so diffuse that even at a large $\alpha$ it can overlap well with the ligand donor orbital. This is an important factor that differentiates the Cp$_2$An chemistry from d transition metal analogues.[26] At the same time d$_\pi$, **10**, starts to participate in the Th–C$^1$ bonding. The d$_\pi$ lobe pointing down in the –$y$ direction expands so as to warrant a good overlap with the distorted-ethyl donor orbital. An effect similar to this d$_\pi$ participation was emphasized in assessing the electronic origin of the deformation of carbene ligands in some Ta complexes,[27a] and methyl tilting in Ti complexes.[27b]

The evolution of the overlap populations is displayed in Figure 6, top. As one would expect from the preceding orbital analysis, the Th–C$^2$ overlap population stays constant for the wide range of $\alpha$, and the flat top of the Th–C$^1$ curve at around $\alpha$ = 140° sits above the Th–C$^2$ curve. Once again evidenced is the bonding ability of the Cp$_2$Th fragment to hold the distorted ethyl group tightly, and the larger Th–C$^1$ overlap population, albeit only slightly, is in harmony with shortening of the Th–C$^1$ bonds in **1**, **6**, and **7**. As $\alpha$ increases, a new interaction turns on. This is between Th and the $\alpha$-hydrogen atoms on C$^1$, **13**. While the
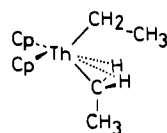


**13**

calculated Th–H$^1$ overlap population is not great, e.g., 0.042 at $\alpha$ = 160°, the agostic interaction should help the C$^1$H$_2$CH$_3$ ligand to deform, and perhaps it is another reason behind the Th–C$^1$ bond shrinkage. To materialize this effect, we bring out the Th–(C$^1$H$_2$CH$_3$) group overlap population (GOP) defined as a sum of all the Th–C and Th–H overlap populations associated with the ethyl ligand. Figure 6, bottom, illustrates its variation, which for comparison provides the Th–(C$^2$H$_2$CH$_3$) GOP as well. Differing from the flat GOP curve for Th–(C$^2$H$_2$CH$_3$), the Th–(C$^1$H$_2$CH$_3$) GOP moves up rapidly with increment of $\alpha$. At $\alpha$ = 160°, the difference amounts to 0.117.

In the course of the extensive distortion of the ethyl (C$^1$H$_2$CH$_3$), we found a σ-electron drift occurring from C$^1$ to Th. Then the

(26) For example, $\eta^2$-acyls in Cp*$_2$An(COR)X and related $\eta^2$-carbamoyls in Cp*$_2$An(CONR$_2$)X can adopt either the O-inside or the O-outside conformations with respect to X, while for the d transition metal analogues, Cp$_2$M(COR)X (M = Ti, Zr), only the O-inside geometry is energetically feasible. The electronic origin of this contrast was traced to the different shapes of the Cp$_2$MX fragment orbitals between group 4 metals and actinides. For details, see ref 3f.

(27) (a) Goddard, R. J.; Hoffmann, R.; Jemmis, E. D. *J. Am. Chem. Soc.* **1980**, *102*, 7667–7676.  (b) Eisenstein, O.; Jean, Y. *Ibid.* **1985**, *107*, 1177–1186.
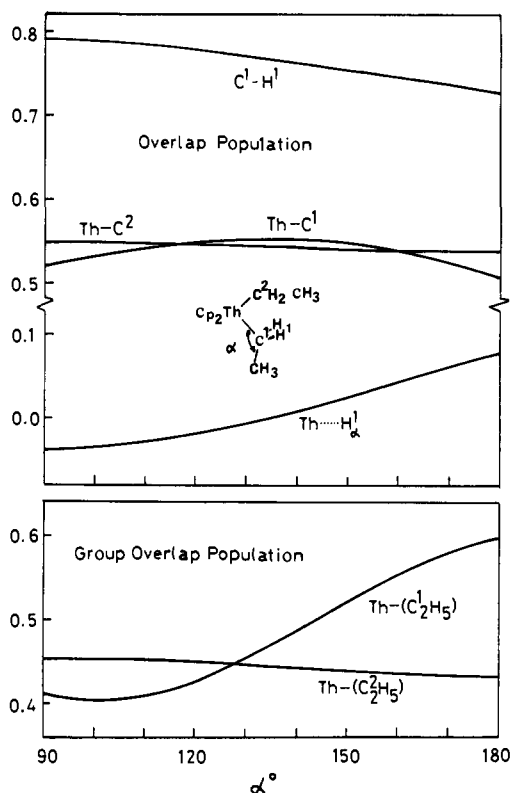


**Figure 6.** Variation of the overlap populations (top) and the Th–ethyl group overlap populations (bottom) in Cp$_2$Th(C$_2$H$_5$)$_2$ as a function of the Th–C$^1$–C angle $\alpha$.
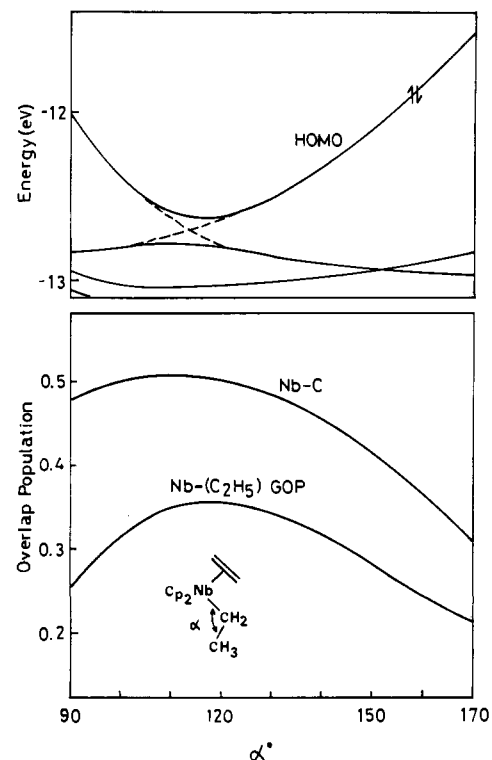


**Figure 7.** (top): Walsh diagram for ethyl pivoting ($\alpha$) in Cp$_2$Nb-(H$_2$C=CH$_2$)(C$_2$H$_5$). (bottom): Variation of the Nb-C overlap population and the Nb-ethyl group overlap population.

C$^1$ atom becomes less negative and thus probably less nucleophilic than the normal ethyl C$^2$ atom (**14**). Also the C$^1$–H$^1$ bond weakens as manifested by the drop of C$^1$–H$^1$ overlap population from 0.778 ($\alpha$ = 120°) to 0.745 ($\alpha$ = 160°). The result is consistent with the long C–H distances in **1**, where these have been determined accurately to be 1.114 (9) and 1.122 (8) Å.
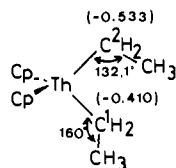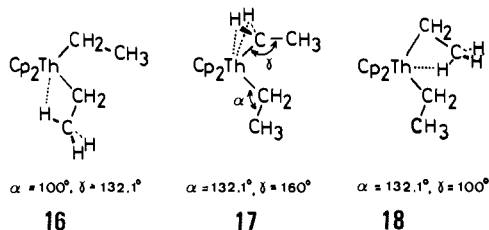
**14**

We turn to $Cp_2Nb(H_2C=CH_2)(C_2H_5)$, a normal ethyl coordination. The $Cp_2Nb(N_2C=CH_2)^+$ fragment orbitals may be easily obtained from the familiar $Cp_2M$ orbitals (M; d metal),[14a,16] or one might refer to the frontier orbitals of $Cp_2TiCl^+$ too.[3f] The major difference of $Cp_2Nb(H_2C=CH_2)^+$ from $Cp_2TiCl^+$ is the absence of a low-lying vacant $d_\pi$, because this orbital is pushed down by the interaction with $H_2C=CH_2$ $\pi^*$ and accomodates two d electrons. Therefore, only the vacant $d_\sigma$ can take care of the $C_2H_5^-$ donor, and **15** draws its orbital shape. Figure 7 gives the
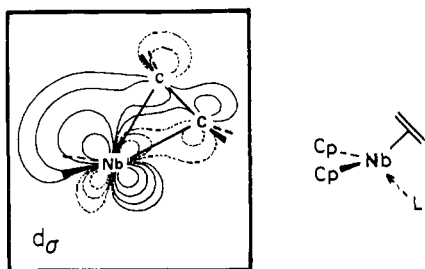
**15**

Walsh diagram and the changes in overlap populations for the ethyl distortion. In contrast to the Th system, the HOMO moves to higher energy as $\alpha$ opens up from the minimum at $\alpha = 115°$, which follows well the total energy change in Figure 4. The Nb–C overlap population curve and the Nb–$(C_2H_5)$ GOP curve both tell us that the Nb–$C_2H_5$ interaction is maximized when the ligand adopts its normal coordination mode. This is traced to the optimal overlap between Nb $d_\sigma$ and the ethyl donor orbital. The $d_\sigma$ lobe pointing toward the incoming ethyl is fairly compact in size compared with the Th $d_\sigma$ lobe, **9**, so that the ethyl ligand in the Nb complex does not enjoy much freedom to choose various orientations. The good interaction is achieved only in the narrow range of $\alpha$ at around 120°.

Before concluding this section, we briefly comment on some other modes of ethyl distortion in $Cp_2Th(C_2H_5)_2$. These are illustrated in **16–18**, which are less stable than **13** by only 0.18,

$\alpha = 100°, \delta = 132.1°$       $\alpha = 132.1°, \delta = 160°$       $\alpha = 132.1°, \delta = 100°$

**16**                 **17**                 **18**

0.19, and 0.42 eV, respectively. The distortion in **17** is similar to that in **13**, and the Th–H overlap population is again positive (0.036). Pivoting an ethyl group in the direction opposite to **13** or **17**, a $\beta$ hydrogen atom comes close to Th as in **16** or **18**. Although we cannot conclude immediately whether or not the Th–$H_\beta$ agostic interaction exists say via a direct Th–$H_\beta$ interaction or via an interaction between Th and $C_\beta$–$H_\beta$ bonding electrons,[28] the evidence here is a slightly positive Th–$H_\beta$ overlap population: 0.036 for **16** or 0.009 for **18**. Whatever the case is, versatility of the ethyl coordination mode means hydrogen atoms (or C–H

bonds) in either the $\alpha$ or the $\beta$ position can approach the actinide center without difficulty. The same would be true for $\gamma$ hydrogens (or $C_\gamma$–$H_\gamma$) when present. This argument should provide a theoretical basis for understanding important aspects of C–H activation and cyclometalation chemistry involving actinide centers.[29]

Interestingly, in the crystal structure of $Yb[N(SiMe_3)_2]_2$-$[Me_2PCH_2CH_2PMe_2]$ there is a short contact between Yb and one methyl group in the $N(SiMe_3)_2$ ligand, **19**.[29c] It was pos-
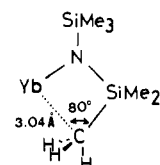
**19**

tulated that the Yb–methyl intteraction was primarily due to a metal–carbon rather than a metal–hydrogen bonding because the methyl hydrogens were located nearly at tetrahedral positions. In the distorted structure of $(CH_3)_2Si\{(CH_3)_4C_5\}NdCH(SiMe_3)_2$ (**8**), a close Nd–methyl contact was also noted.

### Butadiene Coordination to Actinide

Our attention in this section is directed to outlining the electronic details of actinide-to-butadiene bonding, focusing on the following issues: the factors determining the mode of *s-cis*-butadiene coordination that the novel actinide 1,3-diene complexes actually exhibit, and how stable or unstable are their s-trans isomers. It has been known that the 1,3-diene complexes of zirconium, $Cp_2Zr(1,3$-diene$)$, take up either s-cis (**20**) or s-trans (**21**) structures. For example, the two geometrical isomers of
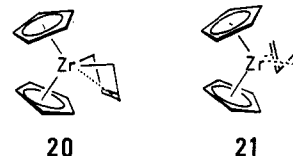
**20**                       **21**

$Cp_2Zr(C_4H_6)$ coexist in a solution in the ratio of s-cis/s-trans 55/45 at 25 °C.[30] The trans structure becomes more favorable as the terminal hydrogens of butadiene are substituted by $CH_3$ or $C_6H_5$, and the X-ray structures are available for $Cp_2Zr(s$-$trans$-$C_4H_6)$[30] and $Cp_2Zr(s$-$trans$-PhHC=CHCH=CPhH).[31] The s-trans coordination was also found in $CpMo(NO)$-$(Me_2C=CHCH=CMe_2)$.[32] Thus one might expect such an s-trans coordination mode to be accessible for the actinide system as well, which will, however, turn out not to be the case.

Analysis here follows the strategy similar to the one employed for our theoretical study of $Cp_2Zr(C_4H_6)$.[33] The model actinide compounds are $Cp_2Th(C_4H_6)$ and $Cp_2U(C_4H_6)$, where all the C–C bond lengths of butadiene are set equal at 1.44 Å as we did for $Cp_2Zr(C_4H_6)$. Upon coordination to a metal, s-cis and s-trans dienes deform in somewhat different ways. To simulate this we chose two geometrical variables $L$ and $\theta$ for the s-cis complex as depicted in **22**. $L$ describes the up-and-down slide of butadiene in the $z$ direction, while the angle $\theta$ defines the swing of inner

(28) For d-metal complexes, metal-$H_\beta$ agostic interactions have occasionally been found: (a) Dawoodi, Z.; Green, M. L. H.; Mtetwa, V. S. B.; Prout, K. *J. Chem. Soc., Chem. Commun.* **1982**, 802–803. (b) Brookhart, M.; Green, M. L. H. *J. Organomet. Chem.* **1983**, *250*, 395–408 and references therein.

(29) (a) See ref 6b and references therein. (b) Simpson, S. J.; Turner, H. W.; Andersen, R. A. *J. Am. Chem. Soc.* **1979**, *101*, 7728–7729; *Inorg. Chem.* **1981**, *20*, 2991–2995. (c) Tilley, T. D.; Andersen, R. A.; Zalkin, A. *J. Am. Chem. Soc.* **1982**, *104*, 3725–3727.

(30) Erker, G.; Wicher, J.; Engel, K.; Rosenfeldt, F.; Dietrich, W.; Krüger, C. *J. Am. Chem. Soc.* **1980**, *102*, 6346–6348.

(31) Kai, Y.; Kanehisa, N.; Miki, K.; Kasai, N.; Mashima, K.; Nagasuna, K.; Yasuda, H.; Nakamura, A. *J. Chem. Soc., Chem. Commun.* **1982**, 191–192.

(32) (a) Hunter, A. D.; Legzdins, P.; Nurse, C. R.; Einstein, F. W.; Willis, A. C. *J. Am. Chem. Soc.* **1985**, *107*, 1791–1792. (b) Hunter, A. D.; Legzdins, P.; Einstein, F. W. B.; Willis, A. C.; Bursten, B. E.; Gatter, M. G. *Ibid.* **1986**, *108*, 3843–3844.

(33) Tatsumi, K.; Yasuda, H.; Nakamura, A. *Isr. J. Chem.* **1983**, *23*, 145–150.
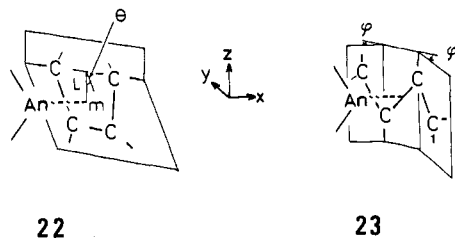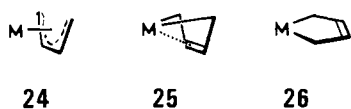
**22**                                    **23**

carbons away from the metal. The fixed An–m separation of 2.0924 Å was so chosen as to set the An–C(terminal) distance as 2.54 Å when $L = 0.0$ Å. For s-trans, the two terminal methylenes were allowed to fold toward An as a function of $\varphi$ in **23**. The An–C(inner) distance of 2.54 Å was kept unchanged.

The total energy calculations on $Cp_2Th(s\text{-}cis\text{-}C_4H_6)$ in terms of the above two geometrical parameters gave a minimum at $L = 0.4$ Å and $\theta = 27°$. Figure 8 presents a cross section of the potential surface at $L = 0.4$ Å, on which is superimposed the potential curve for $Cp_2Th(s\text{-}trans\text{-}C_4H_6)$ as a function of $\varphi$. The total energy curves show that there is a sizable energy gap of 0.74 eV between the s-cis and the s-trans minima ($\varphi = 10°$), in favor of s-cis. A similar energy profile was obtained for the U complexes, $Cp_2U(s\text{-}cis\text{-}C_4H_6)$ and $Cp_2U(s\text{-}trans\text{-}C_4H_6)$. The optimized s-cis geometry ($L = 0.3$ Å, $\theta = 25°$) was again favored over the s-trans ($\varphi = 10°$), but to a somewhat lesser extent (0.42 eV) than the Th case. These results are in contradistinction to the energetics obtained for $Cp_2Zr(C_4H_6)$, where stability of the s-cis and the s-trans isomers are well-balanced, the difference being merely 0.07 eV in favor of s-cis.[33] Incidentally we may remark that the s-trans geometry of $Fe(CO)_3(C_4H_6)$ was calculated to be 1.3 eV higher than the well-known $\eta^4$ s-cis structure. The notable preference for the s-cis ligation in the actinide systems is incarnated in the following experimental facts.

The isolated 1,3-diene complexes of actinides include $Cp^*_2Th(C_4H_6)$ (**2**), $Cp^*_2U(C_4H_6)$, $Cp^*_2Th(CH_2CMeCMeCH_2)$, and $Cp^*_2Th(CPhHCHCHCPhH)$.[7,8] These molecules were prepared by the three distinct routes: (1) $Cp^*_2AnCl_2$ (An = Th, U) + $(THF)_2Mg(CH_2CRCRCH_2)$ (R = H, $CH_3$) or $(THF)_2Mg(CPhHCHCHCPhH)$, (2) $Cp^*_2An(CH_3)Cl$ + Mg-$(CH_2CH_2CH=CH_2)Br$, and (3) $Cp^*_2UCl_2$ + $2LiCH=CH_2$. Route 2 leads to butadiene complexes via an intermediate $Cp^*_2An(CH_3)(CH_2CH_2CH=CH_2)$ and the subsequent methane elimination, an intriguing pathway.[7] Whichever method was used, the product was exclusively an s-cis-diene complex. In the case of $Cp_2M(s\text{-}cis$ diene) (M = Zr, Hf), low-temperature irradiation of the s-cis complexes resulted in formation of the s-trans isomers. However, under similar conditions such an s-cis to s-trans isomerization did not take place when M = Th.[8b] Also low-temperature photoreactions of $Cp^*_2ThPh_2$ with 1,3-dienes did not give any s-trans-diene complexes of Th. Thus there is no evidence so far for s-trans ligation of 1,3-diene to actinide which is relevant to $Cp_2Zr(s\text{-}trans\text{-}CRHCHCHCRH)$ (R = H, Ph). We will analyze the nature of bonding between s-trans diene and actinide later in this section.

Let us take a closer look at the s-cis-diene complexes first. The s-cis coordination mode can vary from the conventional $\eta^4$ (**24**) to $\sigma^2,\pi$ (**25**) to planar 1,4-$\eta^2$ or metallacyclopentene (**26**). The familiar structure of $Fe(CO)_3(C_4H_6)$ represents **24**,[34] while for group 4 and 5 metals the description **25** is a major contribution to the bonding.[30,35] There are no such transition metal complexes



**Figure 8.** Superposition of the two potential energy curves. One is for $Cp_2Th(s\text{-}trans\text{-}C_4H_6)$ as a function of $\varphi$, and the other is for $Cp_2Th(s\text{-}cis\text{-}C_4H_6)$ as a function of $\theta$ ($L = 0.4$ Å). The geometrical variables are defined in **22** and **23**.

as **26**, up to now.[36] The X-ray structure of **2** indicates that the Th–butadiene complexes may fall in the category **25**, according to the reported geometrical parameters.[7] For instance, the butadiene terminal carbons ($C^1$ and $C^4$) sit above the equatorial-girdle plane of $Cp^*_2Th$ by 0.36 and 0.38 Å, and the inner carbons ($C^2$ and $C^3$) sit below the plane by 0.67 and 0.71 Å. Thus the strongest $Th\text{-}C_4H_6$ interactions would and actually do occur to the carbon atoms closest to the equatorial girdle, the terminal carbons in this case. For the theoretically optimized geometry of $Cp_2Th(s\text{-}cis\text{-}C_4H_6)$, $C^{1,4}$ are 0.40 Å ($=L$) above the plane and $C^{2,3}$ are 0.71 Å below, which agree reasonably with the experimental parameters. The difference in Th–C distances defined as $\Delta d = d(Th\text{-}C^{1,4}) - d(ThC^{2,3}) = -0.17$ (3) Å is also consistent with the description **25**. The corresponding $d$ parameters for $Cp_2Zr(s\text{-}cis\text{-}H_2C=CMe\text{—}CMe=CH_2)$ and $Fe(CO)_3(C_4H_6)$ are $-0.297$ (3) and 0.08 (11) Å. An increment of $\Delta d$ means a stronger metal-to-inner carbon bond, and thus a greater contribution of **24** to the bonding. From the larger $\Delta d$ of $Cp^*_2Th(C_4H_6)$ relative to the one for the Zr complex, it appears that the $\sigma^2,\pi$ character is somewhat less pronounced for the Th complex, and the molecule may incline to **24**. And yet the Th structure is still far away from the ideal $\eta^4$ limit.

The orbital interaction diagram for $Cp_2Th(s\text{-}cis\text{-}C_4H_6)$ is given on the left side of Figure 9. At the extreme left $s\text{-}cis\text{-}C_4H_6$ carries four $\pi$ levels. Before we proceed with the analysis, it is appropriate to prescribe explicitly how to count electrons of the butadiene



**24**        **25**        **26**

---

(34) Numerous X-ray structures of the $Fe(CO)_3(1,3\text{-diene})$ complexes are available. See, for example: Riley, P. E.; Davis, R. E. *Acta Crystallogr., Sect. B* **1978**, *34*, 3760-3763. Mills, O. S.; Robinson, G. *Ibid.* **1963**, *16*, 758-761. Cotton, F. A.; Day, V. W.; Frenz, B. A.; Hardcastle, K. I.; Troup, J. M. *J. Am. Chem. Soc.* **1973**, *95*, 4522-4528 and references therein.
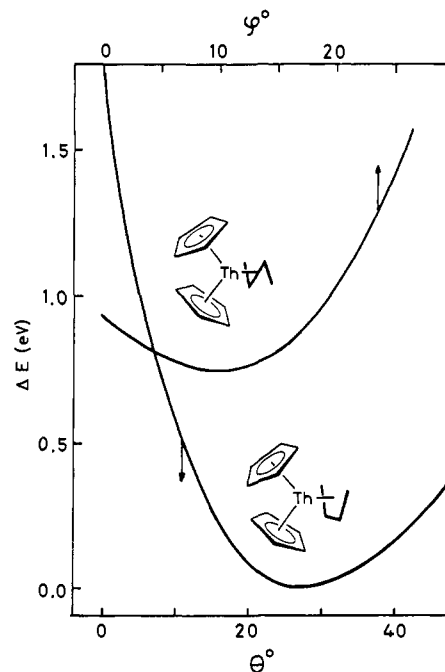
(35) (a) Krüger, C.; Müller, G.; Erker, G.; Dorf, U.; Engel, K. *Organometallics* **1985**, *4*, 215-223. (b) Erker, G.; Krüger, C.; Müller, G. *Adv. Organomet. Chem.* **1985**, *24*, 1-39. (c) Wreford, S. S.; Whitney, J. F. *Inorg. Chem.* **1981**, *20*, 3918-3924. (d) Yasuda, H.; Tatsumi, K.; Okamoto, T.; Mashima, K.; Lee, K.; Nakamura, A.; Kai, Y.; Kanehisa, N.; Kasai, N. *J. Am. Chem. Soc.* **1985**, *107*, 2410-2422. (e) Yasuda, H.; Tatsumi, K.; Nakamura, A. *Acc. Chem. Res.* **1985**, *18*, 120-126. (f) Nakamura, A.; Tatsumi, K.; Yasuda, H. In *Stereochemistry of Organometallic and Inorganic Compounds*; Bernal, I., Ed.; Elsevier: Amsterdam, 1986; pp 1-49.

(36) (a) Putting bulky substituents at the inner carbons in $Cp_2Zr(1,3\text{-di}$ene) enhances the metallacyclopentene character: Erker, G.; Engel, K.; Krüger, C.; Müller, G. *Organometallics* **1984**, *3*, 128-133. (b) There is an interesting report of $Pt(CH_2CMeCMeCH_2)(L_2)$ ($L_2$ = cycloocta-1,5-diene, L = 'BuNC), in which the molecules are thought to have a platinacyclopenta-3-ene structure. Unfortunately their X-ray structures are not available: Barker, G. K.; Green, M.; Howard, J. A. K.; Spencer, J. L.; Stone, F. G. A. *J. Am. Chem. Soc.* **1976**, *98*, 3373-3374.

*Bis(cyclopentadienyl)actinide Complexes*

*J. Am. Chem. Soc., Vol. 109, No. 11, 1987* 3203

ligand. Normally butadiene is viewed as neutral, a four-electron donor. Alternatively we may regard it as a dianionic six-electron donor. The choice is a matter of taste and does not affect the following theoretical results at all. However, the second view looks attractive for the particular Th complex because it sets the Th atom to be an acceptable tetravalent state, and because the metal levels are indeed as high as or higher than the $\pi^*_3$ level. Our choice is $C_4H_6^{2-}$, so that electrons occupy up to the $\pi^*_3$ orbital and the $Cp_2Th^{2+}$ fragment is formally $d^0f^0$ in Figure 9.

Either $\pi^*_3$ or $\pi_2$ interacts very well with metal orbitals. Respectable bonding interactions thus exist between Th and s-cis-$C_4H_6$. The $1a_1$ and $3a_1$ orbitals of $Cp_2Th^{2+}$ interact with $\pi^*_3$. This bonding originates, in effect, from the overlap between Th $x^2 - y^2$ and $\pi^*_3$ (**27**). Also the Th f orbitals, mainly $x(y^2 - z^2)$,[37a] take part in the bonding (**28**). As a result, the Th-$\pi^*_3$ bonding
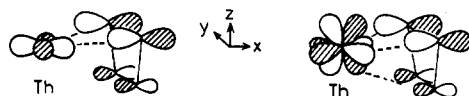


**27**          **28**

molecular orbital (the HOMO) of $Cp_2Th(s$-cis-$C_4H_6)$ contains some contributions from both d (16%) and f (17%) orbitals. However, the major component of the HOMO is the butadiene $\pi^*_3$ orbital itself (61%), implying that the formal electronic configuration of Th in the butadiene complex is close to an $f^0d^0$ tetravalent limit, and involvement of lower formal oxidation states is less important. The bonding partners of $\pi_2$ are $1b_2$ and $3b_2$ of $Cp_2Th^{2+}$. The essence of the interaction lies in the $xy-\pi_2$ overlap (**29**), while the f orbital participation, namely the $yx^2-\pi_2$ overlap (**30**),[37b] is not particularly great. These are incarnated in the metal
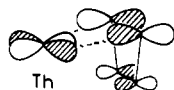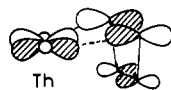


**29**          **30**

composition of the Th-$\pi_2$ bonding molecular orbital, being d (13%) + f (2%). At the lowest energy portion, $\pi_1$ moves up a little partly owing to an antibonding interaction with the inner 6p of Th and partly owing to the complicated mixing with some of the occupied levels of $Cp_2Th^{2+}$.

The uranium-to-butadiene bond is achieved in a way similar to $Cp_2Th(s$-cis-$C_4H_6)$. The butadiene $\pi^*_3$ and $\pi_2$ orbitals interact with $3a_1$ and $3b_2$ of $Cp_2U^{2+}$ (see Figure 1, right), respectively, through overlaps equivalent to **27** and **29**. The f orbital bonding like **28** and **30** is also operative. The major difference between the interaction diagram of $Cp_2U(s$-cis-$C_4H_6)$ (not shown) and the one of $Cp_2Th(s$-cis-$C_4H_6)$ is increased involvement of U f orbitals and concomitant less U d participation, particularly in the U-$\pi^*_3$ bonding. The U-$\pi^*_3$ bonding molecular orbital of the complex contains 6% U d and 48% U f. Despite the appreciably large f population in that orbital, however, we are inclined to consider that the formal oxidation state of U in $Cp_2U(s$-cis-$C_4H_6)$ is still better to be read as tetravalent.

We have calculated metal–carbon(butadiene) overlap populations and charges on the carbon atoms for $Cp_2Th(s$-cis-$C_4H_6)$ and $Cp_2U(s$-cis-$C_4H_6)$. The results are summarized in the upper rows of Table III, which for comparison gives also the corresponding parameters for $Cp_2Zr(s$-cis-$C_4H_6)$ and $Fe(CO)_3(s$-cis-$C_4H_6)$. An important facet of the population analysis is the large overlap population between Th and the terminal carbon atom $C^1$ relative to the Th–$C^2$(inner) overlap population. Their difference, $\Delta P$, may be a convenient index of strength of the $\sigma^2,\pi$ character vs. $\eta^4$ character in bonding. Thus the $\Delta P$ criterion makes a clear

(37) (a) The notation, $f_{x(y^2-z^2)}$, is used according to our choice of the coordination system shown in Figure 9 and **28**. If the $x$ and the $z$ axes are interchanged, the orbital can be read as the more familiar sounding $f_{z(x^2-y^2)}$. (b) By the above axes exchange, $f_{yx^2}$ will become $f_{yz^2}$.

**Table III.** Calculated Overlap Populations (P) and Atomic Charges (Q) for s-Cis and s-Trans Isomers of $Cp_2Zr(C_4H_6)$, $Cp_2Th(C_4H_6)$, and $Cp_2U(C_4H_6)$, and for $Fe(CO)_3(s$-cis-$C_4H_6)$



s-cis          s-trans

| | $P(M-C^1)$ | $P(M-C^2)$ | $\Delta P^a$ | $Q(C^1)$ | $Q(C^2)$ |
|---|---|---|---|---|---|
| | | | s-Cis | | |
| $Cp_2Zr(C_4H_6)^b$ | 0.338 | 0.060 | 0.278 | −0.100 | +0.120 |
| $Cp_2Th(C_4H_6)$ | 0.318 | 0.049 | 0.269 | −0.398 | −0.087 |
| $Cp_2U(C_4H_6)$ | 0.262 | 0.029 | 0.233 | −0.282 | −0.039 |
| $Fe(CO)_3(C_4H_6)^b$ | 0.202 | 0.184 | 0.018 | −0.220 | +0.018 |
| | | | s-Trans | | |
| $Cp_2Zr(C_4H_6)^b$ | 0.204 | 0.164 | 0.040 | −0.029 | +0.072 |
| $Cp_2Th(C_4H_6)$ | 0.184 | 0.095 | 0.089 | −0.443 | −0.080 |
| $Cp_2U(C_4H_6)$ | 0.128 | 0.078 | 0.050 | −0.293 | +0.072 |

$^a \Delta P = P(M-C^1) - P(M-C^2)$. $^b$ From ref 33.

choice in the Th case. The description **25** or the earlier picture of **2** is most appropriate for the mode of diene coordination to Th. $\Delta P$ decreases slightly from Zr to Th, but they are substantially larger than that for $Fe(CO)_3(C_4H_6)$. The trend parallels well the X-ray-derived structure parameter $\Delta d$ mentioned earlier. For $Cp_2U(s$-cis-$C_4H_6)$, $\Delta P$ is still smaller than the Th $\Delta P$, pointing to a weaker $\sigma^2,\pi$ character. The difference in $\Delta P$ is not so great among the Zr, Th, and U complexes that we hesitate to put too much meaning in the $\Delta P$ change. Nevertheless, according to the variable-temperature NMR study, the ring inversion barrier increases in the order $Cp_2Zr(C_4H_6)$ (12.6 kcal/mol)[35a] < $Cp^*_2Th(C_4H_6)$ (15.0) < $Cp^*_2U(C_4H_6)$ (17.0).[7] The ring inversion presumably occurs via a planar metallacyclopentene structure, **31**. Should a larger barrier to this inversion arise from the greater
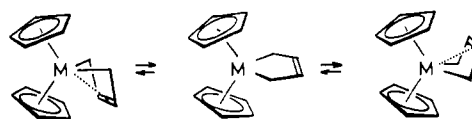


**31**

tetrahapto character of the butadiene bonding, the observed order is surprisingly consistent with the calculated $\Delta P$ change.

Another interesting outcome of the population analysis is the highly negative charge accumulated on the butadiene terminal carbons in the Th and U complexes. The high positioning of the actinide valence orbital levels is a reason as one may see in the interaction diagram of Figure 9. Polarity of the actinide–terminal carbon bonding is intensified for $Cp_2Th(C_4H_6)$, and as a matter of fact the terminal carbon atoms are nearly as negative as the ethyl carbons in $Cp_2Th(C_2H_5)_2$ (**14**). No wonder that $Cp^*_2Th$-$(C_4H_6)$ violently reacts with organic carbonyls and that even an insertion of pyridine into the Th–C(terminal) bond takes place readily at −78 °C leading to the $\pi$-allyl complex, **32**.[8]
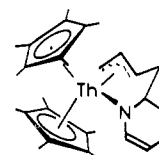


**32**

We return to the energetically unfavorable s-trans-butadiene ligation to actinides. The interaction diagram for $Cp_2Th(s$-trans-$C_4H_6)$ is shown on the right side of Figure 9. The Th–$\pi^*_3$ bonding interaction in the HOMO is less developed than in the s-cis-butadiene complex, and this is the primal cause of the relative instability of the s-trans geometry (see Figure 8). The HOMO level of s-trans is 0.23 eV higher in energy than that of s-cis, so that its contribution to the total energy difference amounts to 0.46
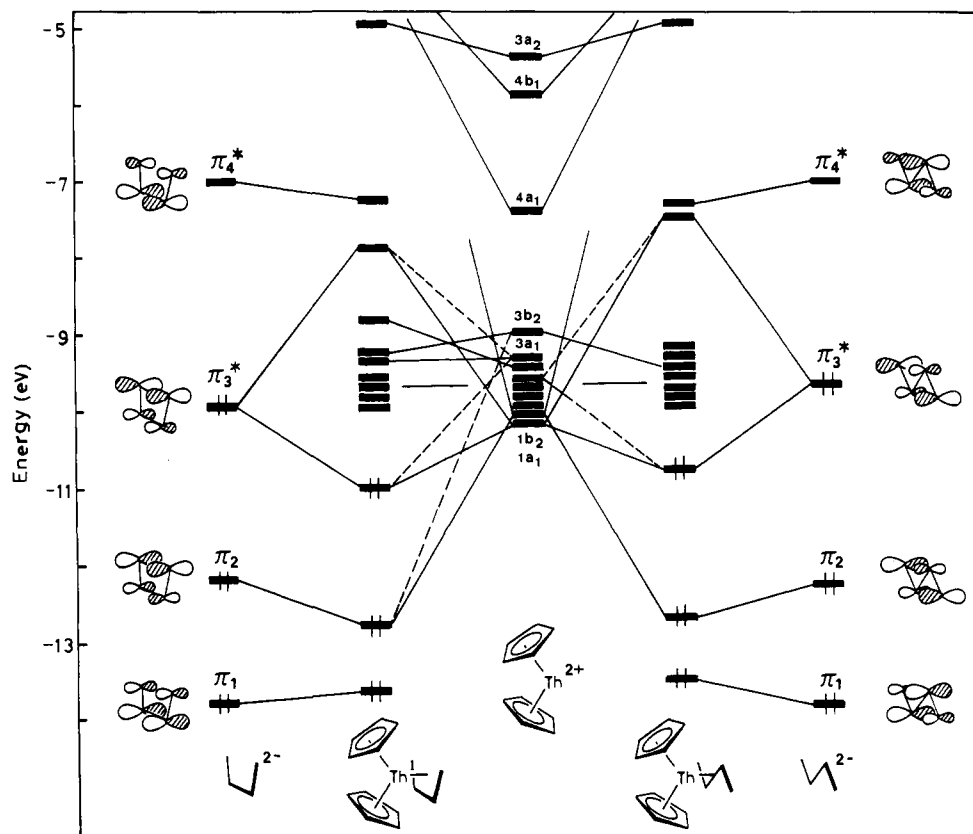
**Figure 9.** Interaction diagram for $Cp_2Th(C_4H_6)$. At left is an s-cis-$C_4H_6$ coordination geometry (L = 0.4 Å, $\theta$ = 27°); at right, an s-trans-$C_4H_6$ coordination geometry ($\varphi$ = 10°). Note that the $Cp_2Th^{2+}$ fragment orbitals should be viewed from a direction which differs from the one in Figures 1 and 5.

eV. In contrast, the $Zr-\pi^*_3$ interactions in $Cp_2Zr(s\text{-}cis\text{-}C_4H_6)$ and in $Cp_2Zr(s\text{-}trans\text{-}C_4H_6)$ were found to be well-balanced.[33] The overlap populations listed in the lower rows of Table III corroborate the energy trend. In the case of Zr, the drop of $P(Zr-C^1)$ in going from s-cis to s-trans is nearly compensated by increase of $P(Zr-C^2)$, and the sum of Zr–C overlap populations for s-trans is comparable to the one for s-cis. Since the inner carbons take part in $ZrC_4H_6$ bonding as much as the terminal carbons do, $Cp_2Zr(s\text{-}trans\text{-}C_4H_6)$ is best represented as **21**, where butadiene may act as linked two $\eta^2$-olefins. For Th, and also for U, $P(An-C^1)$ decreases from s-cis to s-trans, too, but the increase in $P(An-C^2)$ is not as great as the Zr case. The s-trans-$C_4H_6$ ligand does not attain a good bis-$\eta^2$ type interaction with actinides, nor does it maintain a strong $\sigma^2,\pi$ bond. The relatively weak s-trans-$C_4H_6$ coordination is a consequence.

Then where does the difference between the Zr system and the actinide analogues originate from? We think one possible factor is the shape of the $a_1$ symmetry orbital of the $Cp_2M$ fragment which interacts with $\pi^*_3$. The $a_1$ orbital of $Cp_2Zr$ is the $y^2$ type as in **3**, and its overlap with $\pi^*_3$ of s-cis-$C_4H_6$ is not so large and happens to equally match the $a_1-\pi^*_3$ overlap in the s-trans form, **33**. On the other hand, the corresponding $a_1$ orbital of $Cp_2An$



**33**
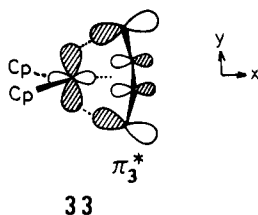
bears an $x^2 - y^2$ character and is substantially diffused as drawn in Figure 1 (the $3a_1$ orbital) and in **24**. The shape of An $a_1$ is suited for an overlap with the s-cis $\pi^*_3$, while it does not fit well with nodal property of s-trans $\pi^*_3$, **34**. The f-orbital participation

through the $x(x^2 - 3y^2)-\pi^*_3$ overlap, **35**, helps, but such an interaction is not sufficiently strong to reverse the relative stability.



**34**          **35**
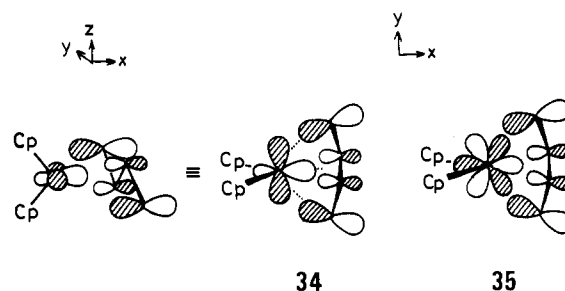
### Actinacyclopentadiene and Cyclobutadiene Coordination

Only a single example of actinacyclopentadiene is available. The reaction of $[Cp^*_2UCl]_3$ with diphenylacetylene has been reported to give $Cp^*_2U(C_4Ph_4)$ (**36**), via oxidative coupling of the



**36**
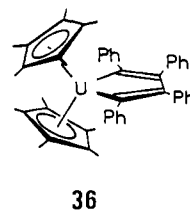
alkyne,[38a] which was also prepared by the sodium amalgam reduction of $Cp^*_2UCl_2$ in the presence of the alkyne or by the route using $Cp^*_2UCl_2$ and 1,4-dilithiotetraphenylbutadiene.[38b-d] Product

(38) (a) Manriquez, J. M.; Fagan, P. J.; Marks, T. J.; Vollmer, S. H.; Day, C. S.; Day, V. W. *J. Am. Chem. Soc.* **1979**, *101*, 5075–5078. (b) Manriquez, J. M.; Fagan, P. J.; Marks, T. J. *Ibid.* **1978**, *100*, 3939–3941. (c) Fagan, P. J.; Manriquez, J. M.; Marks, T. J.; Day, C. S.; Vollmer, S. H.; Day, V. W. *Organometallics* **1982**, *1*, 170–180. (d) See ref 6a.
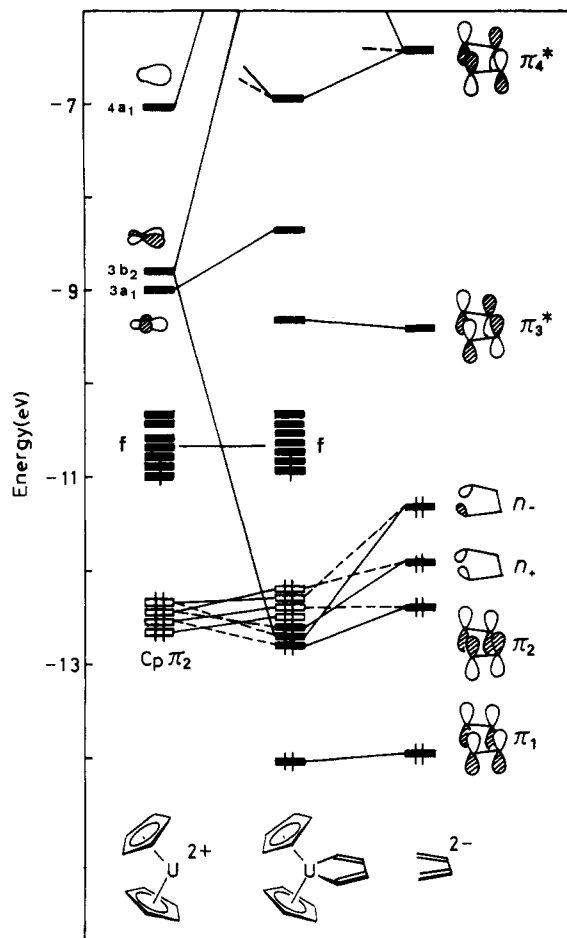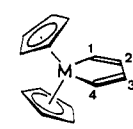
*Bis(cyclopentadienyl)actinide Complexes*

*J. Am. Chem. Soc., Vol. 109, No. 11, 1987* 3205



**Figure 10.** Interaction diagram for $Cp_2UC^1H=C^2H-C^3H=C^4H$. The assumed bond distances for the metallacycle are: $U-C^1$, 2.45 Å; $C^1-C^2$, 1.37 Å; $C^2-C^3$, 1.45 Å. Note that the $Cp_2U^{2+}$ fragment orbitals are viewed from a direction differing from the one in Figure 1.

**36** appears to possess very high thermal stability. There are, however, a good number of such metallacycles of d-transition metals.[39] Among others, $Cp_2Ti(C_4Ph_4)$ and $Cp_2Hf(C_4Ph_4)$ are obvious analogues of **36**. Their X-ray structures exhibit appreciable bond-length alternation in the planar carbon chain,[39b] and no indication of strong $\pi$-delocalization through metal d orbitals. A detailed theoretical study of $Cp_2Ti(C_4H_4)$ has supported this view.[40]

With this structural information in mind, we assumed our model compounds, $Cp_2An(C_4H_4)$, to have short–long–short C–C bonds in their $C_4H_4$ moiety as well. Figure 10 presents the construction of $Cp_2U(C_4H_4)$ from the $Cp_2U^{2+}$ fragment and a $C_4H_4^{2-}$ unit. The overall bonding scheme closely resemble that of $Cp_2Ti(C_4H_4)$. Two of the vacant d orbitals of $Cp_2U^{2+}$, $3b_2$ and $4a_1$, are chiefly responsible for $\sigma$ bonding with the in-phase and out-of-phase combinations of the $C_4H_4^{2-}$ lone-pair orbitals ($n_+$, $n_-$), and the lower $Cp_2U^{2+}$ $3a_1$ orbital is left almost untouched. The high-lying $3a_2$ and $4b_1$ orbitals (not shown in Figure 10, and see Figure 1) as well as the f-block orbitals of the same symmetry are, in principle, capable of overlapping with $\pi_1$ and $\pi_2$ of $C_4H_4^{2-}$, although no immediately obvious strong interactions with the $\pi$ system are seen in the diagram. A $Cp_2U^{2+}$ fragment orbital, which is largely confined to the Cp $\pi_2$, admixes with the $C_4H_4^{2-}$ $\pi_2$ via

(39) (a) Alt, H.; Rausch, M. D. *J. Am. Chem. Soc.* **1974**, *96*, 5936–5937. (b) Atwood, J. L.; Hunter, W. E.; Alt, H.; Rausch, M. D. *Ibid.* **1976**, *98*, 2454–2459. (c) Mague, J. T. *Inorg. Chem.* **1970**, *9*, 1610–1618; *12*, 2649–2654. (d) Gastinger, R. D.; Rausch, M. D.; Sullivan, D. A.; Palenik, G. J. *J. Am. Chem. Soc.* **1976**, *98*, 719–723. (e) Suzuki, H.; Itoh, K.; Ishii, Y.; Simon, K.; Ibers, J. A. *Ibid.* **1976**, *98*, 8494–8500. (f) Pierpont, C. G.; Downs, H. H.; Itoh, K.; Nishiyama, H.; Ishii, Y. *J. Organomet. Chem.* **1977**, *124*, 93–101.

(40) Thorn, D. L.; Hoffmann, R. *Nouv. J. Chim.* **1979**, *3*, 39–45.

**Table IV.** Overlap Populations and Their $\pi$ Components Calculated for the $Cp_2M(C_4H_4)$ Complexes and $C_4H_4^{2-}$



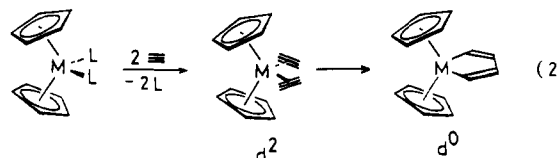| M | Th | U | Ti | metal free |
|---|---|---|---|---|
| $P(M-C^1)$ | 0.634 | 0.610 | 0.437 | |
| $P(M-C^1)$ | 0.104 | 0.092 | 0.052 | |
| $P(M(f)-C^1)_\pi{}^a$ | 0.032 | 0.028 | | |
| $P(C^1-C^2)$ | 1.200 | 1.202 | 1.221 | 1.241 |
| $P(C^1-C^2)_\pi$ | 0.332 | 0.331 | 0.353 | 0.375 |
| $P(C^2-C^3)$ | 0.929 | 0.933 | 0.933 | 0.904 |
| $P(C^2-C^3)_\pi$ | 0.095 | 0.102 | 0.109 | 0.096 |

$^a$The metal f-orbital contribution to $M-C^1$ $\pi$-overlap populations.

U orbitals and via a direct through-space interaction. A full account of the ligand–ligand interaction between Cp and $C_4H_4^{2-}$ was given in the elegant analysis on $Cp_2Ti(C_4H_4)$ and $CpCo-(PH_3)(C_4H_4)$.[40] Because of the complicated interligand mixing, the interaction diagram by itself is not a handy means of judging quantitatively the $An-C_4H_4$ $\pi$ bond strength. The degree of $\pi$-delocalization will be examined based on a population analysis.

Summarized in Table IV are the computed M–C and C–C overlap populations for $Cp_2U(C_4H_4)$, $Cp_2Th(C_4H_4)$, and $Cp_2Ti(C_4H_4)$, together with their $\pi$ components. The basic feature noted in the table is that the metal-to-carbon $\pi$ overlap populations turn out to be moderate in magnitude, after all, for the three metallacycles. The ligand is bound to a metal primarily through $\sigma$ interactions. This result, combined with the fact that the $C^1-C^2$ and $C^2-C^3$ $\pi$ overlap populations differ little from those of the metal-free $C_4H_4^{2-}$, is indicative of weak $\pi$ delocalization occurring in the rings. Interestingly, however, we observed increased M–C overlap populations for the actinide compounds relative to the Ti system. This increment arises partly from somewhat larger An $d-\pi_1,\pi_2$ interactions as **37** and **38**, and partly from the additional weak f bonding through the lovely $xyz-\pi_2$ overlap, **39**. The $f_\pi$ overlap populations, $P(M(f)-C^1)$ $\pi$, would provide an idea to what extent such an f interaction contributes to $An-C$ $\pi$ bonding.



**37**



**38**



**39**

Oxidative couplings of two alkynes coordinated to $d^2$ $Cp_2M$ are known to be symmetry-allowed reactions (eq 2).[14a] One may



$$(2)$$

anticipate that the same will be true for the analogous actinide system, and indeed one synthetic route to the uranacycle, **36**, involves the C–C coupling of diphenylacetylene. However, no convincing evidence is presently available for the formation of stable actinide–alkyne bonds. As an alternative pathway, an electron transfer to alkyne may take place prior to the C–C
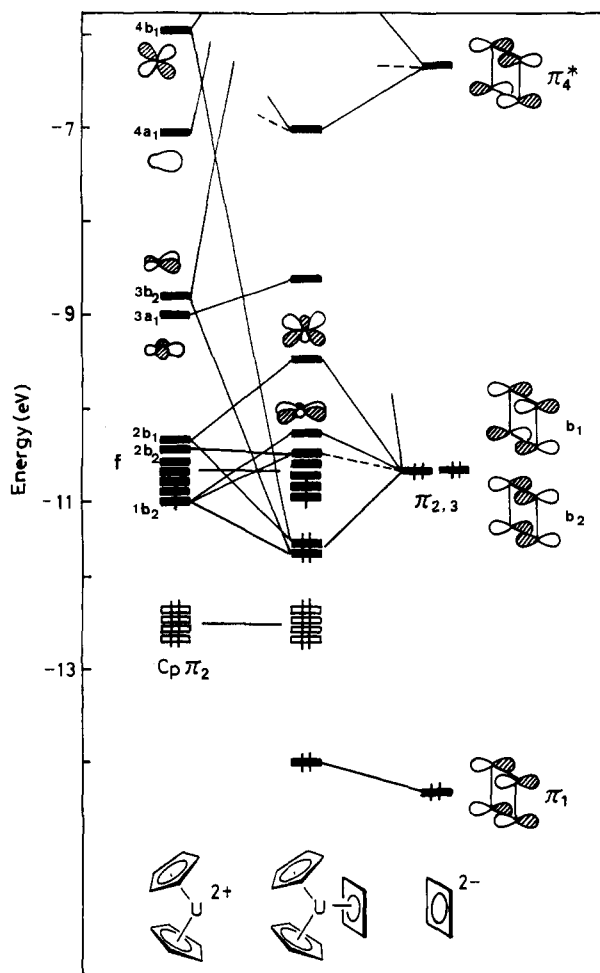
**Figure 11.** Interaction diagram for $Cp_2U(\eta^4\text{-}C_4H_4)$ with the U–C(cyclobutadiene) distance of 2.6 Å.

coupling step. Much remains to be done, both experimentally and theoretically, in order to gain insight into this interesting reaction.

An intriguing isomer of the actinacyclopentadienes would be $Cp_2An(\eta^4\text{-}C_4H_4)$. We know of no authentic example of a cyclobutadiene coordination to actinides, while the beautiful family of actinide complexes of cyclooctatetraenediyl, a related cyclic dianion, is well-known.[41] The cyclo $C_4H_4{}^{2-}$ ligand bears four $\pi$ orbitals, and Figure 11 illustrates how these interact with $Cp_2U^{2+}$ orbitals. In the calculations, we optimized the U–C($C_4H_4$) distance to be 2.6 Å where the hydrogen atoms were bent away from U by 12° with respect to the $C_4$ plane. The $Cp_2U$–$(\eta^4\text{-}C_4H_4)$ bonding is achieved primarily by stabilization of the originally

degenerate $\pi_2$ and $\pi_3$ orbitals. The $\pi_2$ interacts with the $Cp_2U^{2+}$ $3b_2$ and the f-block orbitals of the same symmetry, where the f-orbital participation stems, in essence, from the $yx^2$–$\pi_2$ overlap. Analogously, the bonding partners of $\pi_3$ are $4b_1$ and $zx^2$. These interactions are sketched below in **40–43**. The lower positioning
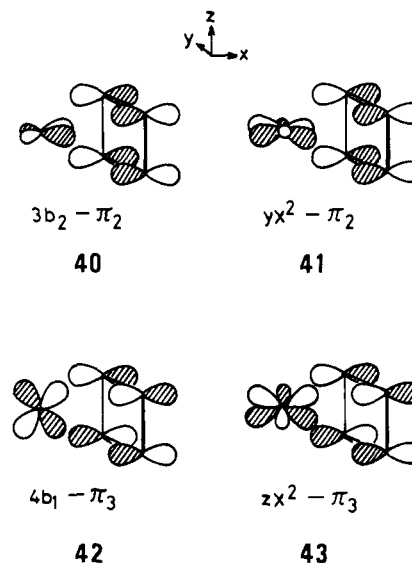


of the $3b_2$ level compared with the $4b_1$ level results in a stronger $3b_2$–$\pi_2$ interaction, while the f bonding occurs more strongly with $\pi_3$. Then the resulting two bonding molecular orbitals, "$\pi_2$" and "$\pi_3$", of $Cp_2U(\eta^4\text{-}C_4H_4)$ happen to be nearly degenerate. The metal orbital components in these bonding orbitals are p (2%) + d (5%) + f (25%) in "$\pi_3$" and p (2%) + d (8%) + f (18%) in "$\pi_2$", consistent with the above interpretation.

It is evident from Figures 10 and 11 that the U–($C_4H_4$) bonding is better attained in the metallacyclopentadiene structure. In fact, $\overline{Cp_2UCH}\!=\!CHCH\!=\!CH$ was computed to be 2.5 eV more stable than $Cp_2U(\eta^4\text{-}C_4H_4)$. Although no doubt the uranacycle is thermodynamically more favorable, we point out that the cyclobutadiene coordination would be kinetically stable, if a suitable synthetic route can be found by the following two reasons. (1) The uranium-to-cyclobutadiene bonding itself is reasonably strong owing to the interactions shown in **40–43**. It is actually stronger than the uranium-to-cyclopentadienyl bonding in Figure 1. The U–C($\eta^4\text{-}C_4H_4$) overlap population is 0.153, which is unquestionably larger than the U–C(Cp) overlap population of 0.072 (av). (2) A C–C bond cleavage of $Cp_2U(\eta^4\text{-}C_4H_4)$ with simultaneously forming two U–C $\sigma$ bonds is symmetry forbidden,[40] and will meet a high-energy barrier on the way to the thermodynamically more stable metallacycle.

(41) (a) Streitwieser, A., Jr.; Müller-Westerhoff, U. *J. Am. Chem. Soc.* **1968**, *90*, 7364. (b) Streitwieser, A., Jr.; Müller-Westerhoff, U.; Sonnichsen, G.; Mares, F.; Morrell, D. G.; Hodgson, K. O. *Ibid.* **1973**, *95*, 8644–8649. (c) Streitwieser, A., Jr.; Kinsley, S. A. In ref 1c, pp 77–114 and references therein.